Case 7 - Dimension reduction in risk analysis

Jan Jonker (i6278777); Ton Vossen (i6280587)
Pénélope Ledunois (i6411508); Gil Schwaller (i6288482)
Joris van der Pas (i6383389)

May 30, 2025

Abstract.
In this study, we develop a concise, multi-stage framework for constructing risk-minimizing portfolios. We first model individual asset volatilities using Realized GARCH with range-based measures, then capture dynamic dependencies via ADCC, and impose sparsity with a covariance graphical lasso. Portfolio weights are derived through Constrained Hierarchical Risk Parity, optimized for out-of-sample Sharpe over a rolling window. Backtests (January 2021–December 2024) show superior risk-adjusted performance versus both minimum-variance and equal-weight benchmarks—even under (more) realistic transaction costs up to $1 bn AUM.

Keywords. risk parity; Realized GARCH; ADCC; graphical lasso; portfolio optimization

Maastricht University

Contents

1 Introduction

From 2021 to 2024, in the post-COVID period, inflation rates increased significantly worldwide. As economies recovered rapidly and demand surged after lockdowns, governments injected substantial liquidity into markets. Meanwhile, energy, gas, and commodity prices spiked due to geopolitical uncertainty. These external shocks created high inflation and market volatility, eroding investor confidence. Despite changing market behaviors, one objective remains constant: constructing portfolios that minimize investment risk. Traditional theories—such as the Global Minimum Variance portfolio introduced by Markowitz (1952)—have inspired countless studies and practitioners but can underperform in volatile or large universes where identifying low-risk assets is challenging.

In this paper, we develop and compute a three-stage portfolio strategy for identifying, evaluating, and investing in the least risky assets from a broad universe. First, we estimate conditional volatilities using a Realized-GARCH model with intra-day proxies. Next, we capture time-varying dependencies via an Asymmetric Dynamic Conditional Correlation (aDCC) framework. Finally, we construct the portfolio using Constrained Hierarchical Risk Parity (DHRP).

Building on the classical minimum-variance framework, we ask: does our multi-stage approach achieve superior risk reduction compared to the traditional minimum-variance portfolio? We address this empirically and then incorporate transaction costs, showing how turnover policy and scale affect net returns and how to mitigate excessive trading.

Our contribution is twofold. First, we demonstrate that combining modern volatility and correlation models with structured allocation via DHRP yields low-risk portfolios in practice. Second, we systematically compare DHRP against conventional methods, emphasizing the critical role of realistic frictions like transaction costs. For transparancy, the code can be found in the footnote.[1]

2 Data Collection

We sourced daily return data from the CRSP database on WRDS, covering the period January 2017 through December 2024. The initial universe comprised 53 large-cap stocks selected to span global markets (primarily U.S. names, but also listings from Europe, Asia and Latin America) and a diverse set of sectors including Technology, Healthcare, Financials and Consumer Goods. After inspecting each series for data integrity (non-numeric entries, missing-values,

[1] Fully implemented in R; complete end-to-end code are available at https://github.com/KoperSloper/EAFM.

etc.), we removed 11 stocks exhibiting excessive gaps, leaving 42 tickers for analysis. Remaining isolated missing values were forward-filled to preserve the time series without introducing look-ahead bias.

3 Realized GARCH, Adaptive DCC and Regularization

3.1 Realized GARCH

Realized GARCH integrates the traditional GARCH approach of Bollerslev (Bollerslev, 1986) with nonparametric high-frequency measures of volatility (the "realized" component) to deliver more efficient and accurate conditional variance estimates (Hansen et al., 2011). In particular, letting r_t denote the return on day t and x_t an observable realized measure (e.g. realized variance constructed from intraday returns), the Realized GARCH(1,1) model is specified by

$$r_t = \sqrt{h_t}\, z_t, \qquad z_t \overset{\text{i.i.d.}}{\sim} N(0,1), \tag{1a}$$

$$h_t = \omega \;+\; \beta\, h_{t-1} \;+\; \gamma\, x_{t-1}, \tag{1b}$$

$$x_t = \xi \;+\; \varphi\, h_t \;+\; \tau(z_t) \;+\; u_t, \quad u_t \overset{\text{i.i.d.}}{\sim} N(0,\sigma_u^2). \tag{1c}$$

Here $h_t = \mathrm{Var}(r_t \mid \mathcal{F}_{t-1})$ with $\mathcal{F}_t = \sigma\{r_s, x_s : s \le t\}$, and equation (1c), often called the measurement equation, links the latent variance to its noisy high-frequency proxy.

A parsimonious yet flexible choice for the leverage function is

$$\tau(z) \;=\; \tau_1\, z \;+\; \tau_2\,(z^2 - 1),$$

which allows for asymmetric ("leverage") effects.

In the absence of high-frequency intraday returns, we adopt the Parkinson (1980) range estimator as our daily realized volatility measure. For each asset i at time t, define

$$x_{i,t} = \sqrt{\frac{\left[\ln(\mathrm{High}_{i,t}/\mathrm{Low}_{i,t})\right]^2}{4\,\ln 2}}.$$

The intuition is that daily returns may fail to capture intraday volatility, especially on days with large price swings that ultimately cancel out. For example, if a stock opens and closes at \$100, the return is zero which would suggest no volatility. But if the price reached \$150 during the day and dropped to \$50

before returning to \$100, substantial volatility clearly occurred. While simple returns would label this a quiet day, the Parkinson's range correctly captures the true extent of the price fluctuations.

3.2 Adaptive DCC

Having established the Realized GARCH framework for the marginal variances, we next describe how to embed it within an Adaptive Dynamic Conditional Correlation (ADCC) (Cappiello et al., 2006) model to capture time-varying correlations across multiple assets.

Once the univariate volatilities h_{it} are estimated, define the standardized residuals

$$\varepsilon_{it} = \frac{r_{it}}{\sqrt{h_{it}}}, \qquad \varepsilon_t = (\varepsilon_{1t}, \ldots, \varepsilon_{Nt})',$$

and let the negative-shock vector be

$$n_t = I(\varepsilon_t < 0) \circ \varepsilon_t,$$

where "$\circ$" denotes the Hadamard product. The ADCC update for the $N \times N$ matrix Q_t is then given by

$$\begin{aligned} Q_t = (&\bar{Q} - A' \bar{Q} A - B' \bar{Q} B - G' \bar{N} G) \\ &+ A' \varepsilon_{t-1}\varepsilon_{t-1}' A + B' Q_{t-1} B + G' n_{t-1} n_{t-1}' G \end{aligned} \tag{2a}$$

$$R_t = Q_t^{*-1} Q_t Q_t^{*-1}, \quad Q_t^* = \operatorname{diag}\big(\sqrt{q_{11,t}}, \ldots, \sqrt{q_{NN,t}}\big). \tag{2b}$$

where

$$\bar{Q} = \frac{1}{T}\sum_{t=1}^{T} \varepsilon_t \varepsilon_t', \quad \bar{N} = \frac{1}{T}\sum_{t=1}^{T} n_t n_t',$$

and A, B, G are diagonal $N \times N$ parameter matrices governing, respectively, news impact, persistence and asymmetric (negative-return) effects. The diagonal normalizer Q_t^* guarantees that R_t has ones on the diagonal and remains a valid correlation matrix.

To avoid lookahead bias, the quantities $\bar{Q}$ and $\bar{N}$ are computed recursively using only past data from the current window. That is, for an update at time t, we set $T = t - 1$, ensuring that Q_t and R_t are based solely on information available up to time $t-1$. We used a moving window of size 1000 days and refit every 5 days.

3.3 Regularization

To obtain a sparse estimate of the covariance matrix Σ, we solve the covariance graphical lasso problem (Bien and Tibshirani, 2011). Specifically, letting S be the sample covariance based on n observations, we estimate

$$\hat{\Sigma} = \arg\max_{\Sigma \succ 0} \left\{ -\frac{n}{2} \left[\log\det(\Sigma) + \operatorname{tr}\big(S\,\Sigma^{-1}\big) \right] \; - \; \big\|\Lambda \circ \Sigma\big\|_1 \right\}. \tag{3}$$

where "$\circ$" (again) denotes the Hadamard product and $\|\cdot\|_1$ the sum of absolute values of all entries. The ℓ_1-penalty $\|\Lambda * \Sigma\|_1 = \sum_{i,j} \lambda_{ij}|\sigma_{ij}|$ induces sparsity by shrinking small covariances exactly to zero, while the constraint $\Sigma \succ 0$ ensures positive definiteness.

Let $S = (S_{ij})$ be the sample covariance matrix and $R = (r_{ij})$ the sample correlation matrix. For a grid of thresholds $\rho_1 < \cdots < \rho_L$ (by default the L quantiles of $\{|r_{ij}|\}$), let's define

$$\Lambda_{ij}^{(\ell)} = \frac{1}{S_{ij}}\, I\big(|r_{ij}| < \rho_\ell\big).$$

For each ℓ we solve (3) and then select the final $\hat{\Sigma}$ by minimizing the BIC. The intuition is that stock pairs with weak correlations are likely to reflect noise, and are therefore penalized heavily and shrunk toward zero. In contrast, pairs with strong sample correlations are treated as informative and receive little or no penalization, allowing their covariance estimates to remain intact.

4 From Covariances to Weights

4.1 Problems with General Minimum Variance

Having obtained a sparse, positive-definite covariance estimate $\hat{\Sigma}$, the next step is to translate it into portfolio weights. A naive General Minimum Variance (GMV) portfolio requires inverting the full $p \times p$ matrix,

$$w^\star \;\propto\; \hat{\Sigma}^{-1}\mathbf{1},$$

which becomes both numerically unstable and computationally burdensome as p grows.

4.2 (Constrained) Hierarchical Risk Parity

Hierarchical Risk Parity (HRP; De Prado, 2016) and its constrained variant (DHRP; Pfitzinger and Katzke, 2019) sidestep these issues by avoiding any large matrix inversion. Instead, they proceed in three stages: first, construct a distance metric from the estimated correlations, and apply hierarchical clustering (e.g. single linkage) to generate a dendrogram. Second, use the clustering tree to sort the assets into a quasi-diagonal order so that highly correlated instruments are placed together. Third, perform recursive bisection on this ordered list: at each split, allocate capital between the two sub-clusters in inverse proportion to their aggregate variances, then recurse within each branch. This "top-down" procedure naturally allocates more weight to clusters (and assets) with lower risk, without ever computing a large-scale inverse.

4.3 Hierachical Clustering

Let's explore the algorithm in a bit more detail. First we are going to explain the clustering part:

To feed into the (D)HRP algorithm, we start from the estimated $N \times N$ correlation matrix

$$R \;=\; \big(\rho_{ij}\big)_{i,j=1}^{N},$$

obtained from our Realized GARCH–ADCC–CovGlasso pipeline. We then build a tree structure in three steps:

1. Correlation-to-distance transform. Define the asset-pair distance

$$d_{ij} = \sqrt{\frac{1}{2}\big(1-\rho_{ij}\big)}, \qquad D = \big(d_{ij}\big)_{i,j=1}^{N}.$$

2. Distance-of-distances. To cluster based on the full correlation structure, compute for each pair of columns of D the Euclidean distance

$$\tilde{d}_{ij} = \sqrt{\sum_{k=1}^{N}\big(d_{k\,i}-d_{k\,j}\big)^2}, \qquad \widetilde{D} = \big(\tilde{d}_{ij}\big)_{i,j=1}^{N}.$$

   Here $\tilde{d}_{ij}$ measures how similarly assets i and j correlate with all others.

3. Agglomerative clustering (single linkage). We begin with each asset in its own singleton cluster, that is, $\mathcal{C}^{(0)} = \{\{1\},\ldots,\{N\}\}$. At iteration t, we compute for every pair of distinct clusters $u, v \in \mathcal{C}^{(t)}$ the inter-cluster

distance

$$\dot{d}(u, v) = \min_{i \in u,\, j \in v} \tilde{d}_{ij}.$$

The closest pair $(u^\star, v^\star)$ is merged into a new cluster $u_{\text{new}} = u^\star \cup v^\star$, and the clustering is updated as

$$\mathcal{C}^{(t+1)} = \left(\mathcal{C}^{(t)} \setminus \{u^\star, v^\star\}\right) \cup \{u_{\text{new}}\}.$$

Distances between the new cluster and all others are recomputed using the same minimum-distance linkage. This process repeats until all assets have been merged into a single cluster, resulting in a binary hierarchical tree (dendrogram).

4.4 Matrix Seriation

Once the dendrogram is complete, we traverse its leaves from left to right to obtain a permutation of the asset indices that places highly correlated instruments adjacent to one another. Applying this ordering to both rows and columns of the covariance matrix $\hat{\Sigma}$ produces a reordered matrix in which clusters of similar assets appear as nearly block-diagonal submatrices, while off-block covariances are considerably smaller.

Figure 1 shows the effect of this leaf-order permutation on a sample covariance matrix. After seriation, we can see three (clear) clusters on the diagonal.

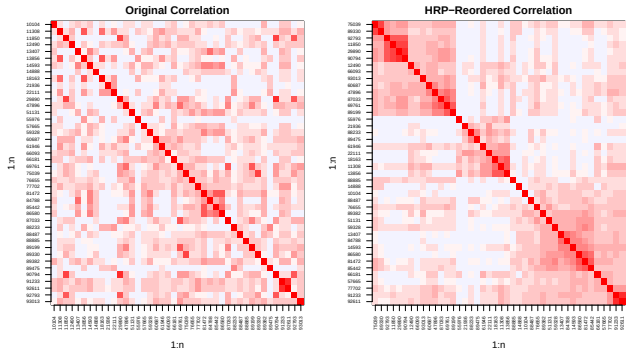

Figure 1: Example of matrix seriation: the original (unordered) covariance matrix on the left vs. the HRP-reordered (quasi-diagonal) matrix on the right. Blocks of highly correlated assets stand out along the diagonal.

4.5 Portfolio Weights

Once the assets have been ordered in quasi-diagonal form by the dendrogram leaf order, we allocate portfolio weights via a top-down recursive bisection. Let N be the total number of assets, indexed by $n = 1, \ldots, N$. Denote by $L = \{L_0\}$ the current list of clusters, with initially

$$L_0 = \{1, 2, \ldots, N\}, \qquad w_n = 1 \ \ (\forall n = 1, \ldots, N),$$

so that every asset starts with equal "raw" weight. Then repeat:

1. Stopping criterion. If every cluster in L is a singleton, i.e. $|L_i| = 1$ for all $L_i \in L$, terminate. At that point the current w_n are the final allocations.

2. Split each non-singleton. For each cluster $L_i \in L$ with $|L_i| > 1$:

   (a) Bisect the cluster. Partition L_i into two sub-clusters

   $$L_i^{(1)} \cup L_i^{(2)} = L_i, \qquad |L_i^{(1)}| = \left\lfloor \tfrac{1}{2} |L_i| \right\rfloor,$$

   preserving the original ordering from the seriation.

   (b) Compute sub-cluster variance. Let $V_i^{(j)}$ be the sample covariance matrix restricted to the assets in $L_i^{(j)}$ (for $j = 1, 2$). Define a unit-normalized weight vector

   $$\widetilde{w}_i^{(j)} = \frac{\operatorname{diag}\big[V_i^{(j)}\big]^{-1}}{\operatorname{tr}\big[\operatorname{diag}(V_i^{(j)})^{-1}\big]},$$

   and then the aggregate variance of each sub-cluster as the quadratic form

   $$\widetilde{V}_i^{(j)} = \widetilde{w}_i^{(j)\prime} V_i^{(j)} \widetilde{w}_i^{(j)}.$$

   (c) Determine the split ratio. Compute

   $$\alpha_i = 1 - \frac{\widetilde{V}_i^{(1)}}{\widetilde{V}_i^{(1)} + \widetilde{V}_i^{(2)}}, \quad 0 \le \alpha_i \le 1.$$

   (d) Rescale allocations. Multiply the current raw weights w_n for each asset $n \in L_i^{(1)}$ by α_i, and for each $n \in L_i^{(2)}$ by $(1 - \alpha_i)$. Formally,

   $$w_n \ \longleftarrow \ \begin{cases} \alpha_i \, w_n, & n \in L_i^{(1)}, \\ (1 - \alpha_i) \, w_n, & n \in L_i^{(2)}. \end{cases}$$

3. Recurse. Replace each processed cluster L_i with its two children $\{L_i^{(1)}, L_i^{(2)}\}$ in the list L, and return to step 1.

After all clusters are singletons, the resulting vector $w = (w_1, \ldots, w_N)$ yields the final HRP allocation.

This method completely avoids the costly and unstable inversion of a full p x p covariance matrix. Only a diagonal matrix must be inverted, which is both trivial and numerically robust.

The only component we adopt from Pfitzinger and Katzke (2019) is the hyperparameter τ, which controls how strictly the algorithm preserves asset similarity when splitting the dendrogram. At $\tau = 0$, symmetry dominates, reproducing the naive bisection from De Prado (2016). At $\tau = 1$, splits follow the original dendrogram exactly, keeping similar assets together. For $0 < \tau < 1$, the algorithm balances both goals: it seeks the most symmetric tree possible without splitting asset pairs that are too similar. Intuitively, τ acts as a height threshold: splits must occur above it, ensuring that clusters remain internally coherent.

4.6 Validation and Hyperparameter Tuning

We use a a walk-forward approach to perform both hyperparameter tuning and out-of-sample testing. Specifically, the only hyperparameter of interest is τ. The idea is to select the value of τ that delivers the best performance in recent history and use it to construct portfolios in the near future.

At each decision point t_0, the model uses the trailing 50 days of data as a validation window. Within this window, candidate values of τ ranging from 0.20 to 0.35 (in increments of 0.05) are considered and evaluated. For each candidate τ, portfolios are constructed using the DHRP method for each of the 50 validation days. The annualized Sharpe ratio is used as the selection criterion, as it seemed to perform the best. That said, other measures like the Sortino ratio could also be considered, especially since the goal is to minimize downside risk.

Once the value of τ with the highest validation Sharpe ratio is found, it is kept fixed for the next 10-day test block. During this period, portfolios are built using the selected τ, and returns are recorded out-of-sample. This setup ensures that the hyperparameter is always chosen based on data available before the evaluation period, which avoids look-ahead bias.

5 Performance, Transaction Costs, and Managing Turnover

We now evaluate the performance of our strategy against two benchmarks: the naive GMV portfolio and the Equally Weighted (EW) portfolio. We begin by analyzing the case without transaction costs. Then, we relax this assumption and examine how different levels of Assets Under Management (AUM) impact performance.

5.1 Performance Without Transaction Costs

Table 1 reports the out-of-sample performance metrics for the DHRP strategy compared to the Naive GMV and EW benchmarks. In the absence of transaction costs, DHRP achieves a Sharpe ratio of 1.024, outperforming both Naive (0.796) and EW (0.903).

While the EW strategy yields a slightly higher annualized return (13.8%) than DHRP (12.9%), this comes with significantly higher volatility. DHRP maintains the lowest volatility (12.6%) and the smallest maximum drawdown (17.6%), reflecting a more stable risk profile. The Sortino ratio, which focuses on downside risk, also favors DHRP (0.095) over Naive (0.074) and EW (0.085).

Table 1: Out-of-sample performance metrics without transaction costs

Strategy	Ann. Return	Ann. Vol	Sharpe	Sortino	Max. Drawdown
DHRP	0.129	0.126	1.024	0.095	0.176
Naive	0.097	0.122	0.796	0.074	0.196
EW	0.138	0.153	0.903	0.085	0.235

Note: Sharpe ratios are computed assuming a zero risk-free rate. The out-of-sample evaluation period spans January 2021 to December 2024.

5.2 Transaction Costs

To capture realistic trading frictions we model the per-dollar transaction cost for stock i at time t as the sum of a linear half-spread component and a nonlinear market-impact term:

$$\mathrm{TC}_{i,t} \;=\; \frac{S_i}{2}\left|D_{i,t}\right| \;+\; \alpha_{i,t}\left|D_{i,t}\right|^{\beta}, \tag{4}$$

where S_i denotes the full bid–ask spread of security i (so that $\frac{1}{2}S_i$ is the half-spread cost per dollar traded) and $D_{i,t}$ is the signed dollar volume traded at time t (positive for buys, negative for sells).

Empirical evidence suggests that market impact scales as a power law in the traded volume, with exponent $\beta \approx \frac{3}{2}$ (Tóth et al., 2011), so we set $\beta = \frac{3}{2}$.

We model the impact coefficient $\alpha_{i,t}$ as

$$\alpha_{i,t} \;=\; c\,\frac{\sigma_{i,t}}{Q_{i,t}^{\beta-1}},$$

where $\sigma_{i,t}$ is the daily return volatility of stock i (taken from the aDCC covariance matrices), $Q_{i,t}$ is its average daily dollar volume, and c is a dimensionless calibration constant (commonly $c = 0.8$) (Grinold and Kahn, 2000).

In this formulation, the first term $\frac{1}{2}S_i\,|D_{i,t}|$ represents the cost of crossing the spread, while the second term $\alpha_{i,t}\,|D_{i,t}|^{\beta}$ captures the nonlinear market impact of large trades.

Stock-specific bid–ask spreads are estimated using the two-day high–low approach of Corwin and Schultz (2012), which infers the proportional spread directly from daily high and low prices. In our implementation, we compute this spread for every trading day and each stock in the dataset, then summarize each security's typical trading cost by reporting the median of its daily spread estimates.

Finally, the total transaction cost incurred by the portfolio at time t is simply the sum across all N assets:

$$\mathrm{TC}_t \;=\; \sum_{i=1}^{N} \mathrm{TC}_{i,t}.$$

5.3 Managing Turnover

To limit excessive trading and contain transaction costs, we impose a threshold rule on both the DHRP and Naive-GMV strategies. Denote by w_t^{target} and w_{t-1}^{prev} the model's suggested weights at rebalancing date t and the actual weights from the previous date. We measure (proposed) turnover as

$$\mathrm{Turn}_t = \sum_{i=1}^{N} \big|\, w_{t,i}^{\text{target}} - w_{t-1,i}^{\text{prev}} \,\big|.$$

If $\mathrm{Turn}_t > \theta$, we rebalance fully to w_t^{target}, incur transaction costs per (4), and set $w_t^{\text{actual}} = w_t^{\text{target}}$. Otherwise (i.e. $\mathrm{Turn}_t \le \theta$) we skip trading and carry forward $w_t^{\text{actual}} = w_{t-1}^{\text{prev}}$.

By contrast, the equal-weight (EW) benchmark resets to $w_i = 1/N$ every $R = 25$ trading days regardless of interim turnover. On non-rebalancing days

weights drift, and on each 25^{th} day we compute transaction costs and reset

$$w_t^{\text{actual}} = \left(\tfrac{1}{N}, \ldots, \tfrac{1}{N}\right).$$

Turnover control is essential: without it, both DHRP and Naive-GMV trade excessively, driving transaction costs so high that net returns collapse. We set the threshold at $\theta = 0.8$ (where 1 represents full turnover) because values in $[0.5, 1.0]$ all substantially reduce costs with negligible performance loss. Tuning θ more precisely remains a straightforward way to extract additional gains.

5.4 Performance Under Transaction Costs

To study the impact of transaction costs at scale, we "simulate" how portfolio performance changes with varying levels of AUM. Intuitively, as AUM increases, performance should deteriorate: larger AUM leads to larger trade sizes, i.e., higher values of $D_{i,t}$, which in turn drive up transaction costs (and especially market impact costs).

We evaluate performance at four AUM levels: \$1 million, \$1 billion, \$100 billion, and \$1 trillion. Table 2 shows that our DHRP model delivers strong risk-adjusted returns when AUM is relatively small. At \$1 million and \$1 billion, DHRP achieves the highest Sharpe ratios (0.944 and 0.932, respectively) and competitive absolute returns, outperforming both Naive-GMV and the equal-weight (EW) benchmark. As AUM increases to \$100 billion, however, DHRP's Sharpe ratio drops to 0.702 (below EW's 0.791), indicating that larger asset pools inflate trade sizes (and thus transaction costs) enough to erode the model's advantage. At \$1 trillion, this effect becomes more pronounced: DHRP's Sharpe plunges to 0.224, while EW still delivers 0.653, so the simple equal-weight rule outperforms DHRP once turnover costs dominate. In short, DHRP is particularly effective at smaller scales, but its relative edge diminishes (and even reverses) at very high AUM levels as transaction costs bite hardest.

6 Discussion

Our empirical analysis shows that enhancing traditional portfolio-construction techniques with enhanced volatility estimates, time-varying correlations, and sparse covariance regularization—embedded within a Constrained Hierarchical Risk Parity (DHRP) framework—yields clear advantages in a frictionless setting. In particular, DHRP delivers the lowest out-of-sample maximum drawdown, while consistently achieving the highest Sharpe and Sortino ratios relative

Table 2: Performance metrics for DHRP, Naive-GMV and EW across four AUM levels

AUM	Strategy	Ann. Return	Ann. Vol	Sharpe	Sortino	Max. Drawdown
$1 million	DHRP	0.118	0.125	0.944	0.088	0.187
	Naive	0.109	0.128	0.850	0.080	0.222
	EW	0.130	0.152	0.857	0.082	0.236
$1 billion	DHRP	0.116	0.125	0.932	0.087	0.187
	Naive	0.105	0.128	0.816	0.077	0.222
	EW	0.129	0.152	0.850	0.081	0.237
$100 billion	DHRP	0.091	0.129	0.702	0.066	0.185
	Naive	0.052	0.146	0.353	0.034	0.222
	EW	0.120	0.152	0.791	0.076	0.243
$1 trillion	DHRP	0.035	0.158	0.224	0.023	0.325
	Naive	-0.052	0.224	-0.230	-0.007	0.373
	EW	0.099	0.152	0.653	0.064	0.257

Note: Sharpe ratios are computed assuming a zero risk-free rate. The out-of-sample evaluation period spans January 2021 to December 2024.

to both the Naive GMV and EW benchmarks.

When realistic transaction costs are introduced, the performance hierarchy shifts but remains favorable to DHRP at typical institutional scales. For AUM levels between $1 million and $1 billion, DHRP maintains its edge across all key metrics—volatility, Sharpe, Sortino, and drawdown.

However, as AUM grows into the $100 billion–$1 trillion range, nonlinear market-impact effects and higher absolute trade sizes begin to erode these benefits. Here the simplicity and minimal rebalancing frequency of the EW strategy outperforms DHRP on a net basis. This outcome highlights a critical trade-off: while more complex models can unlock superior risk-adjusted returns at modest scales, they may incur prohibitive execution costs when deployed with very large capital.

In summary, DHRP offers a powerful blueprint for risk-focused portfolio construction under moderate trading frictions, but practitioners must carefully calibrate model complexity against the scale of funds managed.

7 Limitations and Future Research

7.1 Limitations

Despite the strong empirical performance of our DHRP-based portfolio strategy, several important caveats warrant a candid discussion. First, our linear plus power-law transaction-cost model (4) provides only a rough approxima-

tion of true trading frictions: in practice, bid–ask spreads and market impact evolve stochastically, can exhibit time-varying skewness, and depend on the specific execution algorithms (e.g. iceberg orders or VWAP schedules) used by large traders. Second, we infer daily spreads via the Corwin–Schultz two-day high–low estimator; while computationally convenient, this proxy can be noisy and may misestimate costs. Third, the binary turnover-control rule we implement (Turnover $> \theta$) enforces a "hard" rebalance decision, which may discard useful information contained in the proposed weights. Fourth, although our walk-forward validation protocol guards against lookahead bias, the model still contains many estimated parameters, meaning overfitting cannot be ruled out. Finally, we abstract away from a host of real-world frictions—margin requirements, discrete lot sizes, finite liquidity depth and tick-size effects—which can collectively increase turnover, slippage and financing costs.

7.2 Future Research Directions

A natural extension is to enforce turnover via an explicit ℓ_1 constraint that moves the portfolio as close as possible to the target weights w^* without exceeding a maximum total trade θ. At each rebalancing date we would solve

$$\begin{aligned} \hat{w}_t = \arg\min_{w} \; & \frac{1}{2} \left\| w - w^* \right\|_2^2 \\ \text{subject to} \quad & \sum_{i=1}^{N} \left| w_i - w_{t-1,i} \right| \; \leq \; \theta, \\ & \sum_{i=1}^{N} w_i = 1, \\ & w_i \geq 0, \quad i = 1, \ldots, N. \end{aligned}$$

Here w^* denotes the raw DHRP weights and w_{t-1} the previous portfolio. The ℓ_1 constraint $\sum_i |w_i - w_{t-1,i}| \leq \theta$ directly caps total turnover, while the objective $\frac{1}{2}\|w - w^*\|_2^2$ ensures the new weights remain as faithful as possible to the model signal.

Another relatively straightforward improvement would be to refine the calibration of the turnover threshold parameter, θ. Our results indicate that the degradation in performance at higher AUM levels could potentially be mitigated by making θ adaptive rather than fixed. Specifically, one could define a turnover threshold function $\theta(\text{AUM})$ that decreases with increasing AUM. This would reflect the fact that higher levels of capital are more sensitive to transaction costs and market impact, and therefore require stricter control over turnover. By

reducing θ as AUM increases, the strategy could maintain cost-efficiency and preserve its risk-adjusted advantages at scale.

Beyond turnover control, future work could compare alternative volatility estimators—such as realized variance from intraday data or (for example) the unbiased estimator from Zhang et al. (2005)—and extend the framework to larger asset universes and stress regimes (e.g. the 2008 crisis) to assess scalability and robustness under extreme market conditions.

References

Bien, J. and Tibshirani, R. J. (2011). Sparse estimation of a covariance matrix. *Biometrika*, 98(4):807–820.

Bollerslev, T. (1986). Generalized autoregressive conditional heteroskedasticity. *Journal of Econometrics*, 31(3):307–327.

Cappiello, L., Engle, R. F., and Sheppard, K. (2006). Asymmetric dynamics in the correlations of global equity and bond returns. *Journal of Financial Econometrics*, 4(4):537–572.

Corwin, S. A. and Schultz, P. (2012). A Simple Way to Estimate Bid-Ask Spreads from Daily High and Low Prices. *The Journal of Finance*, 67(2):719–760.

De Prado, M. L. (2016). Building Diversified Portfolios that Outperform Out of Sample. *The Journal of Portfolio Management*, 42(4):59–69.

Grinold, R. C. and Kahn, R. N. (2000). *Active portfolio management : a quantitative approach for providing superior returns and controlling risk*.

Hansen, P. R., Huang, Z., and Shek, H. H. (2011). Realized GARCH: a joint model for returns and realized measures of volatility. *Journal of Applied Econometrics*, 27(6):877–906.

Markowitz, H. (1952). PORTFOLIO SELECTION*. *The Journal of Finance*, 7(1):77–91.

Parkinson, M. (1980). The extreme value method for estimating the variance of the rate of return. *The Journal of Business*, 53(1):61.

Pfitzinger, J. and Katzke, N. (2019). A constrained hierarchical risk parity algorithm with cluster-based capital allocation. Working Paper 14/2019, Stellenbosch University, Department of Economics. Stellenbosch Working Paper Series No. WP14/2019.

Tóth, B., Lempérière, Y., Deremble, C., De Lataillade, J., Kockelkoren, J., and Bouchaud, J.-p. (2011). Anomalous price impact and the critical nature of liquidity in financial markets. *Physical Review X*, 1(2).

Zhang, L., Mykland, P. A., and Aït-Sahalia, Y. (2005). A tale of two time scales. *Journal of the American Statistical Association*, 100(472):1394–1411.